CRYSTAL GROWTH & DESIGN

Article

pubs.acs.org/crystal

Multitechnique Experimental Insight on an Unusual Crystal-to-Crystal High Temperature Solid State Reaction in Zirconium Carboxypyridinephosphonates: From One-Dimensional Chains to Two-Dimensional Hybrid Layers Through HF Elimination

Ferdinando Costantino,[†,⊥] Paola Sassi,[†] Marco Geppi,[‡] and Marco Taddei*[,†]

[†]Department of Chemistry, University of Perugia, Via Elce di sotto n. 8. 06123 Perugia, Italy

[‡]Department of Chemistry and Industrial Chemistry, University of Pisa, Via Risorgimento 35 - 56126 Pisa, Italy

[⊥]ICCOM-CNR, Area di Ricerca CNR, Firenze, Via Madonna del Piano 10, 50019 Sesto Fiorentino, Italy

Supporting Information

ABSTRACT: Two novel *N*-phosphonoethylcarboxypyridines were prepared via nucleophilic substitution of two carboxypyridines (namely, 4-carboxypyridine, or isonicotinic acid, and 3-carboxypyridine, or nicotinic acid) with diethyl-2-bromoethylphosphonate in water. Two zirconium derivatives of these acids were obtained under mild solvothermal conditions, and their structures were solved from powder X-ray diffraction (PXRD) data. The zirconium derivative containing the isonicotinic moiety (**1**), with formula $ZrF_2(HF)(O_3PCH_2CH_2NC_5H_4CO_2)$, has a one-dimensional (1D) chain structure in which the carboxypyridine groups are placed in the external part of the inorganic chain constituted of zirconium octahedra and phosphonic tetrahedra, whereas the zirconium derivative containing the nicotinic moiety (**2**), with formula $ZrF_2(O_3PCH_2CH_2NC_5H_4CO_2)$, has a hybrid layered structure in which zirconium octhaedra and phosphorus tetrahedra form a new structural archetype, with a C−O group coordinating the zirconium atoms. **1** underwent a high temperature (280 °C) slow solid state transformation that involved the loss of one HF molecule coordinated to the zirconium atom and the replacement of this coordination vacancy with the neighboring $C-O^-$ group belonging to the adjacent chain. The structure of this heated compound (**1a**) is a polymorph of **2**. A multitechnique approach, based on coupled Fourier transform infrared spectroscopy and Raman and solid state NMR spectroscopy allowed us to carry out a thorough characterization of these materials, finding nice agreements on the chemical details of this solid state reaction.

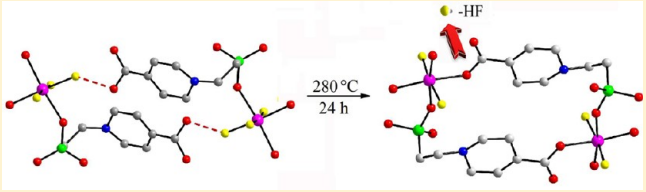

INTRODUCTION

The chemistry of zirconium phosphonates has its roots in the 1970s, but still today, after more than 30 years, it continues to give rise to a remarkable interest in the scientific community, not only from a fundamental point of view, but also for the extent of applications in which they are still employed.[1]

A peculiar feature of these materials resides in their considerable chemical and thermal stability accompanied with a high structural variability. The latter is mainly due to the ease of modulating their structure and reactivity through the rational choice of the phosphonic building blocks. Such double characteristics have been recognized, both in the past and still today, as a fundamental aspect for their application in several fields like proton conductivity, heterogeneous catalysis, fillers for polymeric composites, thin films, and so on.[2]

The ways to assemble zirconium atoms and polyphosphonic groups are almost countless because the capability of phosphonate groups of acting as mono- or divalent and mono-, di-, or tridentate ligands, and the presence of noncovalent interactions, such as H-bonds and hydrophobic/-philic interactions, play a crucial role in building up structural architectures with very different dimensionality and connectivity.

In the last years an important contribution to this chemistry was given by our research group with the publication of several zirconium derivatives with one-, two-, and three-dimensional (1D, 2D, and 3D) structures based on aminomethylenephosphonic acids obtained from the reaction of aliphatic amines, phosphorous acid, and formaldehyde.[3]

Alternatively, phosphonic groups can be covalently linked to aromatic heterocycles (such as pyridines, pyrazoles, and similar molecules) by using a method based on the nucleophilic substitution of these ones on diethyl 2-bromoethylphosphonate in aqueous medium and subsequent acid hydrolysis. This reaction produces a charged quaternary nitrogen atom balanced by a counterion (normally Cl^- or Br^-, depending on the acid used for hydrolysis) which could be incorporated into the structure. Pioneering studies in similar systems have been

Received: July 23, 2012
Revised: September 14, 2012

   dx.doi.org/10.1021/cg301042y | *Cryst. Growth Des.* XXXX, XXX, XXX−XXX

carried out by Vermeulen and co-workers in the beginning of 1990s, when a series of zirconium phosphonates containing pyridine and viologen groups have been prepared and their photophysical and photocatalytic properties studied in fine detail.[4]

In the present paper we report the synthesis of two novel phosphono-carboxylate ligands carried out by the reaction of diethyl 2-bromoethylphosphonic with 3-carboxypyridine (nicotinic acid) and 4-carboxypyridine (isonicotinic acid). The molecular formula of these two novel ligands is $[H_2O_3PCH_2CH_2NC_5H_4CO_2H]^+Cl^-$ (H_3L^1 for isonicotinic and H_3L^2 for nicotinic) and their structures are depicted in Chart 1.

Chart 1. Molecular Formulas of Chloride Salts of H_3L^1 and H_3L^2

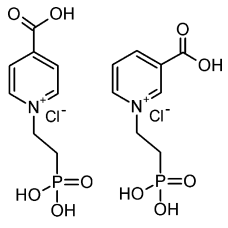

H_3L^1 H_3L^2

Two zirconium derivatives of $[H_3L^1]$ and $[H_3L^2]$ were synthesized under mild solvothermal conditions, and their structures were solved ab initio from powder X-ray diffraction data (PXRD). By reacting $[H_3L^1]$ with zirconium in hydrofluoric acid media, a compound with formula $ZrF_2(HF)(L^1)$ (hereafter **1**) was obtained, which shows a 1D chain structure constituted of an inorganic backbone of ZrO_3F_3 octahedra and PO_3C tetrahedra and with the pending aromatic isonicotinic groups hydrogen-bonded to the adjacent chains. The reaction of $[H_3L^2]$ with zirconium yielded a compound with formula $ZrF_2(L^2)$ (hereafter **2**), having a layered hybrid structure in which the layers are constituted by 1D chains of ZrO_4F_2 octahedra and PO_3C tetrahedra with a connectivity never observed before, linked to each other through the carboxylate groups of the nicotinic moieties.

When heated at 280 °C, **1** underwent a very slow structural transformation that was triggered by the loss of one of the fluorine ligands linked to zirconium as HF, with the consequent formation of a coordination vacancy on the zirconium sphere and the subsequent condensation of two adjacent chains through the formation of a new Zr−O bond filling the coordination vacancy. This new compound (**1a**) is a perfect polymorph of **2**, despite the important differences of the inorganic chain connectivity.

Useful information about the structural transformation observed by PXRD was provided by a thorough investigation by means of solid-state Fourier transform infrared (FT-IR) spectroscopy, Raman, and NMR spectroscopy, especially focusing on the local environment of the zirconium atom. The data collected by means of these techniques were in excellent agreement with the observations from PXRD, thus allowing us to have a detailed picture of the structural features of the investigated compounds.

EXPERIMENTAL SECTION

Reagents. $ZrOCl_2·8H_2O$ was a Merck Pro Analysi product. All the other chemicals were purchased from Sigma-Aldrich.

Synthesis of the Phosphonic Acids. The *N*-phosphonoethyl-4-carboxypyridinium chloride (H^3L^1) was synthesized by modifying the procedure reported in the literature:[4a,b] One gram of isonicotinic acid (8.1 mmol) was mixed with 15 mL of NH_3 0.54 M (8.1 mmol), and 3 g of diethyl-2-bromoethylphosphonate (12.1 mmol) was added to this solution. The mixture was heated at 90 °C for 6 days, and then 15 mL of 12 M HCl was added and the mixture was left reacting for another day. At the end of the reaction the solvent was evaporated under a vacuum and the residue was treated with isopropanol. A white solid precipitated and was filtered. This solid was a mixture of NH_4Cl and H^3L^1, for a total weight of 1.7 g. Titration of the solid with NaOH revealed that the amount of H^3L^1 in this mixture was 70% (1.191 g). Yield: 55%.

^{1}H NMR (D_2O, 400 MHz): δ = 8.96 (d, 2H, aromatic, 2,6-position), 8.34 (d, 2H, aromatic, 3,5-position), 4.78 (m, 2H N−CH_2-), 2.32 (m, 2H, −CH_2−P) ppm. ^{31}P NMR (D_2O, 400 MHz): δ = 19.32 (m) ppm.

The *N*-phosphonoethyl-3-carboxypyridinium chloride (H^3L^2) was prepared with a similar procedure, except for the workup of the product: after evaporation of the solvent, the residue was treated with a 9:1 isopropanol/anhydrous ethanol mixture. A white solid precipitated and was filtered. This solid was a mixture of NH_4Cl, 3-carboxypirydinium chloride, and H^3L^2, for a total weight of 1.5 g. Titration of the solid with NaOH revealed that the amount of H^3L^2 in this mixture was 66% (0.990 g). Yield: 46%.

^{1}H NMR (D_2O, 400 MHz): δ = 9.4 (s, 1H, aromatic, 2-position) 9.03 (d, 1H, aromatic, 6-position), 8.94 (d, 1H, aromatic, 4-position), 8.13 (m, 1H, aromatic, 5-position) 4.85 (m, 2H N−CH_2-), 2.37 (m, 2H, −CH_2−P) ppm. ^{31}P NMR (D_2O, 400 MHz): δ = 18.92 (m) ppm.

Synthesis of the Zirconium Derivatives. Zr derivatives of H_3L^1 and H_3L^2 of formula $ZrF_2(HF)(PO_3CH_2CH_2NC_5H_4CO_2)$ (hereafter **1**) and $ZrF_2(PO_3CH_2CH_2NC_5H_4CO_2)$ (hereafter **2**), respectively, were prepared as follows: 5 mL of a clear solution of the phosphonic acid (0.5 mmol) were mixed with a solution obtained by mixing $ZrOCl_2·8H_2O$ (0.5 mmol) and 0.7 mL of HF 2.9 M (2 mmol). These solutions were maintained in closed plastic vessels for 3 days at 80 °C. The solids obtained were filtered under a vacuum, washed with water, and dried in an oven at 70 °C. Yields (calculated on Zr): 71% for **1**, 53% for **2**.

Analysis: Calcd for $ZrPC_8F_3NO_5H_{10}$ (**1**) Zr = 23.95%, P = 8.15%, F = 14.99% . Exp: Zr = 23.43%, P = 7.88%, F = 16.6%. Calcd for $ZrPC_8F_2NO_5H_9$ (**2**) Zr = 25.33, P = 8.86%, F = 10.58%. Exp: Zr = 24.09, P = 8.68%, F = 9.75%.

Thermal Synthesis of 1a. Compound **1a** was obtained by heating compound **1** at 280 °C for 24 h in a platinum crucible. During this time the structural transformations were followed by PXRD. The thermal treatment was concluded only when the peaks belonging to the pristine phase completely disappeared.

Analytical and Instrumental Procedures. The zirconium and phosphorus contents of the samples were obtained by inductively coupled plasma optical emission spectroscopy using a Varian Liberty Series II instrument working in axial geometry, after mineralization of the samples with hydrofluoric acid.

The fluorine content was determined as fluoride by ion chromatography: about 0.1 g of sample was refluxed for 3 h with 10 mL of 1 M NaOH up to complete hydrolysis. The resulting solution was filtered, properly diluted, and analyzed with a Dionex series 2000 i/sp instrument, using an IonPack AS4A column and a buffer solution, of the following composition: 1.7×10^{-3} M in $NaHCO_3$ and 3.5×10^{-3} M in Na_2CO_3 as eluent.

PXRD patterns for structure determinations and Rietveld refinements were collected with a PANalytical X'PERT PRO diffractometer equipped with a X'Celerator solid state fast detector in the 3−100° 2θ range and with a 30 s/step counting time.

dx.doi.org/10.1021/cg301042y | *Cryst. Growth Des.* XXXX, XXX, XXX−XXX

Thermogravimetric analyses (TGA) were performed using a Netzsch STA490C thermoanalyzer under a 20 mL min^{-1} air flux with a heating rate of 5 °C min^{-1}.

Raman spectra were excited using red radiation from a He−Ne laser; the laser power on the sample was always less than 5 mW. Backscattering illumination and collection of the scattered light were made through an Olympus confocal microscope MOD BX40 (50x and 100× objectives). When a 1800 lines mm^{-1} grating was used, a spectral resolution of about 2 cm^{-1} was achieved. Spectral measurements were made with continuous scans in the range 200−1800 cm^{-1}, exposure times in the range 30−60 s, and 10 accumulations. Detection of scattered light was accomplished by a 1024 × 128 CCD array, mod. SPECTRUM-ONE by Horiba - Jobin Yvon. Calibration of the spectrometer was accomplished using the Raman lines of a polystyrene standard.

Mid-FT-IR measurements were carried out with a Bruker TENSOR27 spectrophotometer composed of a globar source, a high throughput patented RockSolid cube corner interferometer, a deuterated L-alanine tryglycine sulfate detector and a KBr beamsplitter. Transmission spectra were collected at room temperature in the 400−4000 cm^{-1} range. Each spectrum was the average of 50 scans, measured with a resolution of 2 cm^{-1}. The samples were dispersed into anhydrous KBr pellets.

Solid state NMR spectra were recorded on a two-channel Varian Infinity Plus 400 spectrometer working at 400.03 and 376.37 MHz for ^{1}H and ^{19}F nuclei, respectively, equipped with a cross-polarization magic angle spinning (CP-MAS) probe bearing 3.2 mm (outer diameter) rotors. ^{1}H and ^{19}F 90° pulse durations were 2.1 and 3.6 μs, respectively. Optimized relaxation delays of 5 and 30 s were used, and a number of scans of 16 and 40 were accumulated for ^{1}H and ^{19}F, respectively. ^{1}H spectra were recorded using a single-pulse experiment, while the Hahn Echo pulse sequence was used for ^{19}F MAS experiments with an echo delay of 15 μs. Spectra at different MAS frequencies were recorded between 5 and 23 kHz. The chemical shift scales of ^{19}F and ^{1}H spectra are referenced to the signals of $CFCl_3$ and TMS, respectively. All the spectra were recorded at 21 °C.

Structure Determination and Refinement for 1, 1a, and 2. A preliminary profile fit was conducted on the diffraction patterns of **1**, **1a**, and **2** using a split Pearson VII profile function. The position of the first 20 lines (Kα1 maxima) was determined and used for indexing with the *TREOR90*[5] program. Space groups were assigned on the basis of a systematic comparison of the number of peaks found and the number of possible peaks, within all space groups of the respective crystal symmetry, using the *Chekcell*[6] program.

Notably, the cell volume of **2** is twice than that of **1** despite the similarities of the two compounds in terms of molecular weight. As a matter of fact, the asymmetric unit of **2** found after the structure determination process is also doubled, and there are eight formula units per unit cell. Several attempts to find a reduced cell failed and the structure was determined by using the larger unit cell.

The structures of the three compounds were solved using global optimization methods (*FOX*[7] program). The *FOX* program is able to optimize in direct space the molecules described in terms of bond lengths and angles. Optimization is performed over a cost function, in our case the integrated R_{wp}. The reverse Montecarlo parallel tempering algorithm[8] was used, and antibump distances between metals and other atoms were also added. A ZrO_6 octahedron with distances Zr−O of 2.05 Å with standard deviations of 0.05 Å was used. The molecules of H_3L^1 and H_3L^2 ligands were described in terms of bond lengths and angles set at their literature values with standard deviations of 0.15 Å and 10°, respectively. For the structural determination of **1a** several trials in tetragonal symmetry have been performed, but no reliable structural model has been found. The real structure has been found using the pseudotetragonal cell with monoclinic symmetry whose cell parameters are shown in Table 1.

Structural refinement of **1**, **1a**, and **2** was performed using the Rietveld method implemented in the *GSAS*[9] program. Cell parameters, sample displacements, background, and profile were first refined, and then atomic coordinates and atomic displacement parameters were also refined. Soft restraints were used for bond distances and angles.

Table 1. Structural Parameters and Refinement Details for 1, 1a, and 2

compound	1	1a	2
empirical formula	$ZrPC_8F_3NO_5H_{10}$	$ZrPC_8F_2NO_5H_9$	$ZrPC_8F_2NO_5H_9$
formula weight	378.28	358.28	358.28
crystal system	monoclinic	monoclinic	monoclinic
space group	$P2_1/a$	$P2_1/a$	$P2_1/a$
a (Å)	14.2649(3)	12.8478(9)	17.6407(8)
b (Å)	12.8066(2)	12.8510(5)	13.0625(6)
c (Å)	6.6816(1)	6.6366(6)	9.9599(5)
β (deg)	102.447(3)	90.386(9)	97.727(6)
volume (Å^3)	1191.93(4)	1095.7(1)	2274.2(2)
Z	4	4	8
T (°C)	25	25	25
calc density/ cm^{-3}	2.06	2.12	2.04
no. of data	6764	6577	6640
no. of reflections	3643	3802	3386
no. of variables	80	62	132
no. of restraints	40	65	132
R_p	0.054	0.068	0.046
R_{wp}	0.076	0.094	0.063
R_{F^2}	0.103	0.145	0.109
χ	3.33	4.84	8.85

The statistical weight of these restraints was decreased as the refinement proceeded. For **1** the atomic displacement parameters were refined constraining the program to apply the same shift except Zr atoms, whereas those of **1a** and **2** were not refined. At the end of the refinement, the shifts in all parameters were less than their standard deviations.

RESULTS AND DISCUSSION

Crystallography. Crystal data and details of the refinement for **1**, **1a**, and **2** are reported in Table 1. Figure 1 shows the final Rietveld and difference plots.

The structure of **1** is depicted in Figure 2. It has a 1D chain structure built from an inorganic macro-unit constituted of PO_3C tetrahedra and ZrO_3F_3 octahedra running along the *c*-axis. This unit is constructed by the repetition of a four-membered ring of P−O−Zr−O−P atoms that can be also intended as a composite building unit (hereafter CBU) of two Zr octahedra and two P tetrahedra. The same connectivity was observed in other zirconium phosphonates, namely, the zirconium *N*,*N*′-bis(phosphonoethyl)-4,4′-bipyridinium (Zr−P2Viologen)[4b] and more recently in two zirconium amino-phosphonates containing piperidine and bis-piperidine groups.[3f] Each phosphonic tetrahedron is triply connected to three different zirconium atoms, and each zirconium is thus connected to three oxygen atoms belonging to three different phosphonic groups and to three terminal fluorine atoms. Two fluorine atoms are placed in axial position, with the third one occupying the equatorial plane in a *mer* (or trans) reciprocal configuration.

The isonicotinic groups are placed in the external part of the chain through the linking phosphonoethyl groups and, because of the disposition of the phosphonic tetrahedra, they are also alternatively placed up and down with respect to the plane defined by the zirconium atoms. Each COO group of the isonicotinate points toward an adjacent chain and one of the two carboxylate oxygens is near an equatorial fluorine of the

dx.doi.org/10.1021/cg301042y | Cryst. Growth Des. XXXX, XXX, XXX−XXX

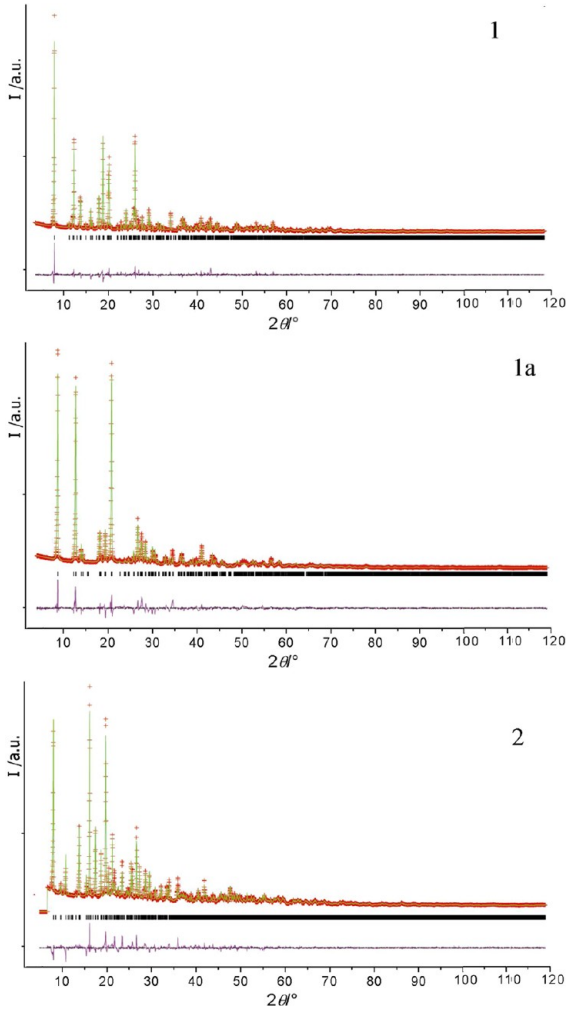

Figure 1. Rietveld plots for **1**, **1a**, and **2**.

neighboring Zr octahedra with a distance of C8−O4···F2 of 2.67(2) Å. This short distance strongly suggests that a noncovalent interaction is present between these two atoms or, more precisely, that F is protonated by the COOH group. PXRD data do not provide any information about the position of the hydrogen atom involved in this interaction, but useful information can be derived from the IR, Raman, and NMR data that will be discussed later. Adjacent chains are linked to each other through these noncovalent interactions and lie along the *a*-axis. No guest species have been found from different Fourier calculations suggesting that no place is available among the chains. In particular, there are no extraframework counterions balancing the positive charge on the nitrogen atoms, since this role is played by the deprotonated carboxylic groups.

The structure of **2** is depicted in Figure 3. It has a layered structure and the layers are constituted by the assembly of inorganic macro-units linked to each other, along the layer plane, by the nicotinic groups. This linkage is allowed by the coordination on zirconium atoms of oxygen atoms belonging to the carboxylic groups so that zirconium octahedra have three oxygen atoms coming from the phosphonic tetrahedra, one from the carboxylic group and two terminal fluorine atoms in *cis* position. The structure of the inorganic macrounit (see Figure 4) is, to the best of our knowledge, observed for the first time, and it can be considered as a new archetype of Zr octahedra and P tetrahedra assembly.

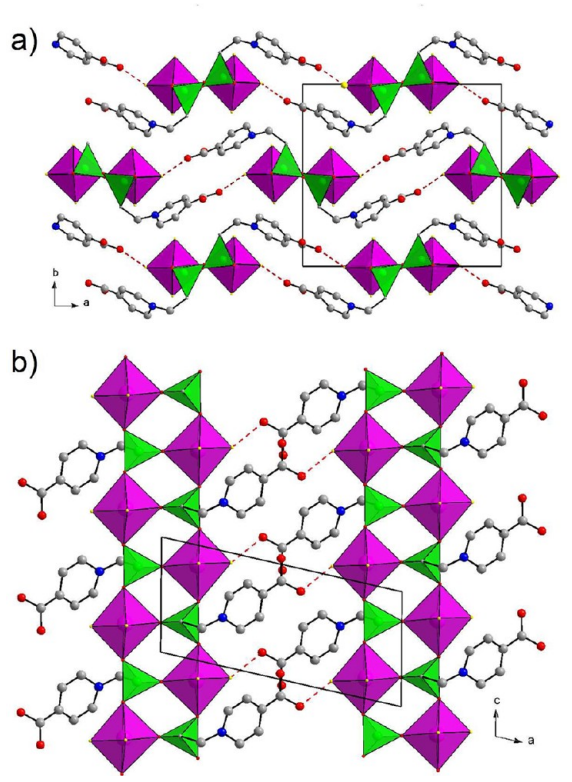

Figure 2. Polyhedral representation of the structure of **1** viewed down the *c*-axis (a), and a detail of a single layer (b). ZrO_3F_3 octahedra are represented in purple, and PO_3C tetrahedra are represented in green. Hydrogen bonds are represented as red dashed lines.

Tetrahedra and octahedra are assembled as follows: there are the same composite building units of compound **1** (represented in light blue in Figure 5), defined by a four-membered ring, which are staggered up and down in a corrugated fashion (Figure 4a,b). The main difference with respect to **1** (Figure 4c) is that in this compound the CBUs are connected through the equatorial oxygen atoms of the zirconium sphere, and the two zirconium atoms of each CBU are crystallographically and chemically equivalent. For **2**, the CBUs are connected through the apical oxygen atoms of Zr octahedra. Moreover, these are not equivalent for symmetry and the asymmetric unit is twice that of **1.** This difference can be ascribed to the *cis*- disposition of the F atoms, one of which (F2 in the case of Zr1 and F4 in the case of Zr2) occupies in **2** the same position occupied by an oxygen atom of the P-tetrahedra and therefore breaks the propagation of the CBU along the *c*-axis, forcing a corrugated disposition.

Like in **1**, also in **2** the nicotinic groups are placed in the external part of the chains, but, at variance with **1**, the chains are covalently linked to each other by means of the bond between the carboxylate group and the zirconium atom. In fact, such a bond substitutes the noncovalent C−O···F interaction found in compound **1**. As a consequence, in this compound the counterion balancing the positive nitrogen is represented by the ZrO_4F_2 complex, bearing a formal negative charge. Notably, no examples of zirconium carboxyphosphonates obtained by direct synthesis with a carboxylic group coordinating the zirconium atom existed up to now: the only example reported with such a feature was obtained by postsynthetic reaction.[3b]

The above-described structural features bring a global structure in which the layers have a considerable thickness

dx.doi.org/10.1021/cg301042y | *Cryst. Growth Des.* XXXX, XXX, XXX−XXX

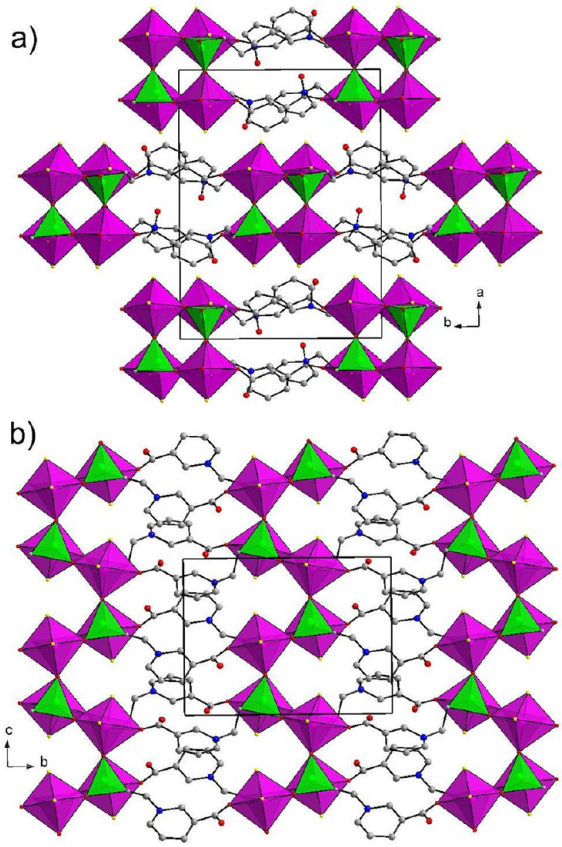

Figure 3. Polyhedral representation of the structure of **2** viewed down the *c*-axis (a), and a detail of a single layer (b). ZrO_4F_2 octahedra are represented in purple, and PO_3C tetrahedra are represented in green.

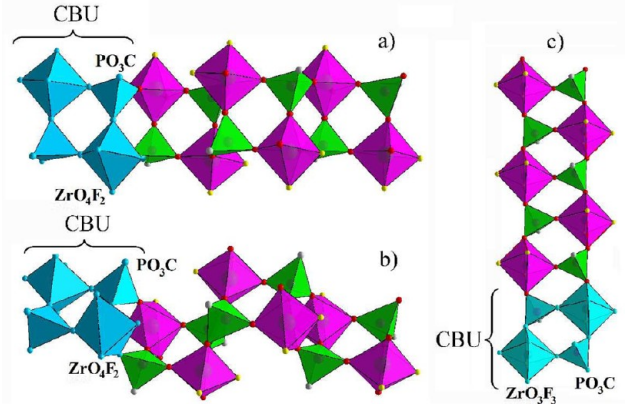

Figure 4. Details of the chain propagation of the CBUs for compound **2** (a and b) and for compound **1** (c) for comparison. The CBUs are represented by the light blue polyhedra.

and are stacked with an *ABA* disposition. Moreover, the layer surface exposes alternate regions of F atoms and aromatic groups suggesting a very resistant thermal behavior (as observed from TG data) and a strong hydrophobic character.

Thermal Behavior. Figure 5 shows the coupled TG curves of **1** and **2**. Both compounds show a remarkable thermal stability.

1 does not lose weight up to about 280°: above this temperature a weight loss is observed corresponding to a small plateau ending around 400 °C. This weight loss can be ascribed to the evaporation of 1 mol of HF/mol of compound (calcd. 5.3%, obs. 5.4%). Beyond this temperature a broad weight loss is observed (calcd 51.3%, obs. 50.3%) due to the combustion of the organic part. We can assume that at the end of the analysis (1200 °C) an equimolar mixture of ZrO_2 and ZrP_2O_7 is formed because the P/Zr molar ratio is 1 in both compounds.

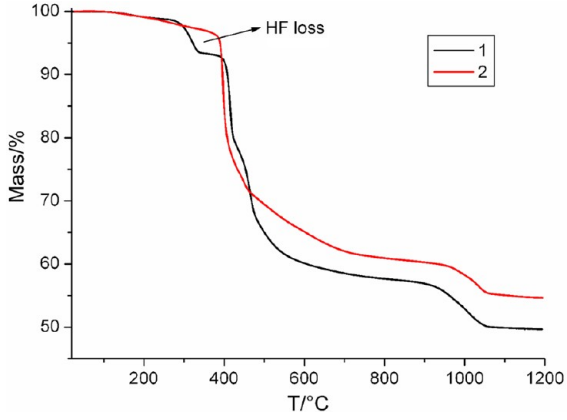

Figure 5. TG curves of compounds **1** and **2**.

The thermal behavior of **2** is very similar to that of **1**. The only difference that can be found is the lack of the weight loss around 280 °C, due to the HF in **1**. This behavior is in a very good agreement with the structural features described above. (Weight loss: calcd 45.9%, obs 45.3%.)

Structure of ***1a****.* The plateau observed in the TG curve of **1** at 280 °C induced us to study what happened around that temperature.

As remarked above, this weight loss can be ascribed to the evaporation of one HF molecule per formula unit. The transition is irreversible and yields the stable crystalline compound **1a**. This result was also confirmed by the ion chromatography analysis on the two solids, which displayed a decrease of the F/Zr ratio from 3 (in **1**) to 2 (in **1a**). The high quality of the diffraction pattern of **1a** allowed us to solve the structure. The structure of **1a** is shown in Figure 6.

The loss of the HF molecule left a coordination vacancy in the zirconium octahedron, and therefore it was saturated by the neighboring oxygen atom O4 belonging to a carboxylate group coming from the adjacent chain. An analogous reaction occurred in a previously reported zirconium derivative,[3b] but the structure of the new phase was not solved, though there were several instances clearly supporting this behavior. The reaction is shown in better detail in Figure 7. Remarkably, similar topotactic transformations on metal carboxyphosphonates involving the loss of water molecules were recently reported by the Demadis-Aranda groups.[10]

The oxygen atom O4, which replaces F2, forms a new bond with the Zr center re-establishing the octahedral coordination (Zr−O4 = 2.08(1) Å). As a consequence, the counterion balancing the positive charge on the nitrogen atom is represented by the ZrO_4F_2 octahedra, bearing a formal negative charge, as in **2**.

This solid state reaction is quite slow (the complete transformation requires about 24 h) and can also be followed by looking at the cell parameters changes. The *a*-axis (parallel to the chain linkage) changes from 14.24 to 12.84 Å, becoming very similar to the *b*-axis (12.86 Å). The new cell found has a pseudotetragonal symmetry, but a reliable structural model in this symmetry was not found. The new obtained compound **1a**

dx.doi.org/10.1021/cg301042y | *Cryst. Growth Des.* XXXX, XXX, XXX−XXX

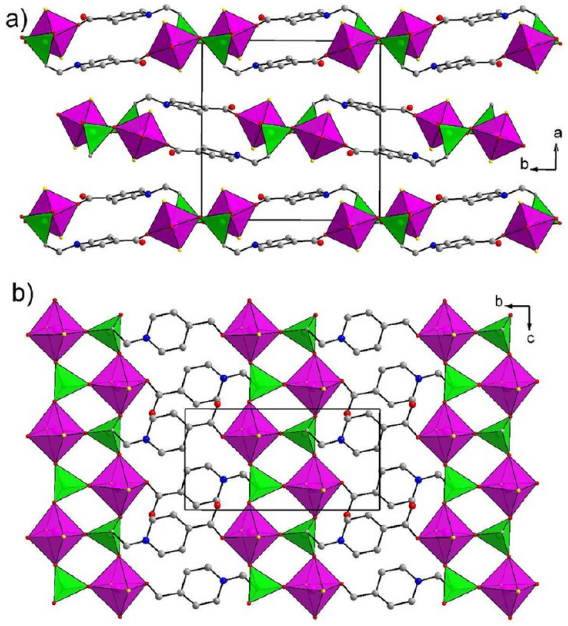

Figure 6. Polyhedral representation of compound **1a** viewed down the *c*-axis (a), and a view of one layer (b). ZrO_4F_2 octahedra are represented in purple, and PO_3C tetrahedra are represented in green.

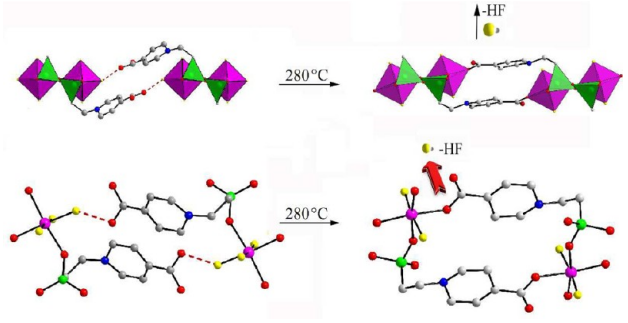

Figure 7. Details of the transformation of **1** into **1a**.

is also a perfect polymorph of **2**: the two compounds have in fact the same composition and molecular weight.

Spectroscopy. The characterization by means of vibrational (infrared and Raman) and NMR spectroscopies was mainly carried out to obtain useful information on the local environment of the octahedral Zr complexes, especially on the arrangement of the fluorine atoms. This also gave us the possibility to describe in fine detail the mechanism of the solid state reaction occurring in **1** to yield **1a**. Figure 8 reports the structure of the octahedral complexes in each compound: the fluorine atoms were labeled as F_α, F_β, and F_γ to allow a clear and unambiguous discussion of all the reported data.

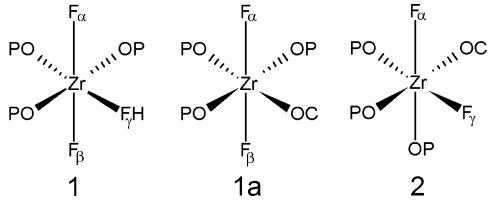

Figure 8. Schematic representation of the octahedral complexes present in **1**, **1a**, and **2**.

FT-IR and Raman. The FT-IR and Raman spectra are shown in Figures 9 and 10, respectively.

The general aspect of IR spectra displays the characteristic absorptions of nicotinic and isonicotinic compounds. A composite system of bands characterizes the 1300−800 cm^{-1} absorptions; due to the superposition of phosphate and

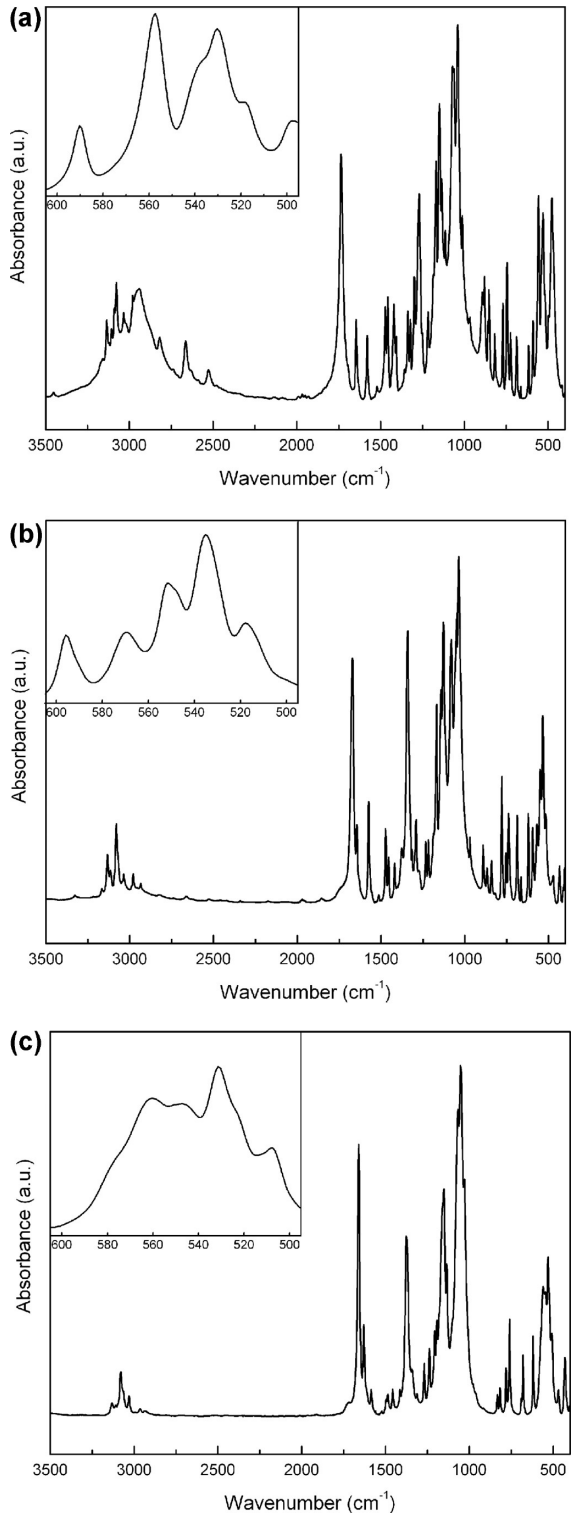

Figure 9. The IR spectra of **1** (a), **1a** (b), and **2** (c). For each compound an inset showing the region between 500 and 600 cm^{-1} is included.

dx.doi.org/10.1021/cg301042y | *Cryst. Growth Des.* XXXX, XXX, XXX−XXX

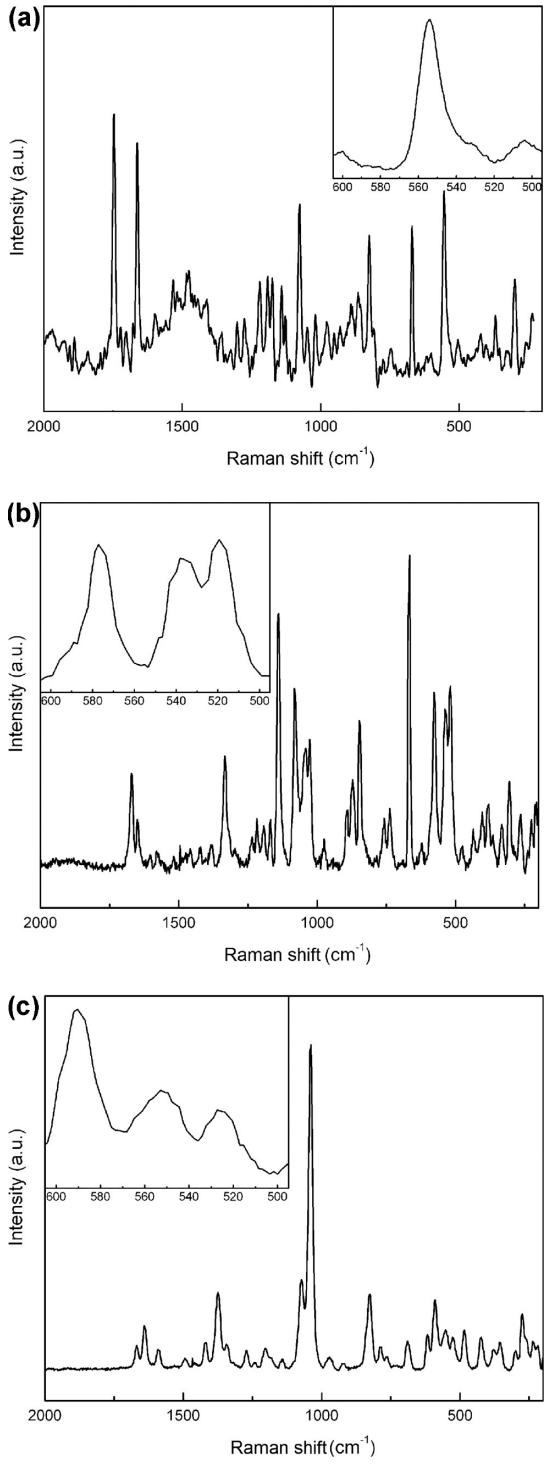

Figure 10. The Raman spectra of **1** (a), **1a** (b), and **2** (c). For each compound an inset showing the region between 500 and 600 cm^{-1} is included.

pyridine modes of vibration, an intense profile is observed in this spectral region.[3f,11,12] Except for this range and despite the variety of signals, some clear indications are derived for the coordination of the zirconium atom. Together with aromatic and aliphatic CH stretching absorptions, the 3100−2800 cm^{-1} spectral region highlights the presence of the intense signal of HF ligand for **1** (absorption at 2942 cm^{-1} in Figure 9a): this band is not revealed for **1a** and **2**, thus confirming the loss of HF ligand. The C═O and C−O stretching modes at 1736 and 1270 cm^{-1}, characteristic of carboxylic acids, are observed in the IR spectrum of **1**. In **1a**, a clear indication of unidentate carboxylate binding to Zr atom comes from the shift of both C═O and C−O vibrations to 1671 and 1341 cm^{-1}, respectively. A similar effect is also evidenced by the Raman spectra of these compounds thus confirming the results of IR detection. In **2**, the vibrational pattern of the carboxylate ligand is at 1660 and 1370 cm^{-1}: again, these signals are both IR and Raman active. The reduced separation between stretching bands of double and single CO bond probably suggests that a higher strength of interaction with Zr atom is established in **2** with respect to **1a**. Indeed, a stronger delocalization of the electronic charge on the metal atom can cause a weakening of the double bond together with a strengthening of the single CO bond: this would result in a red-shift and a blue-shift of relevant stretching signals, respectively.

The low frequency region of Raman spectrum is particularly efficient at revealing the number and type of Zr−F bonds, and also the point symmetry of the metal coordination structure. In fact, according to the *mer*-ZrO_3F_3 octahedral structure (point symmetry C_{2v}), the scattering profile of **1** shows the 551.5 cm^{-1}, 530 cm^{-1}, and 504.3 cm^{-1} bands, assigned to the stretchings of the three Zr−F bonds (see Table 2).[13] The 504.3 cm^{-1} signal is due to the vibration involving the central fluorine atom: it is not observed for **1a**. Conversely, in this sample, the asymmetric and symmetric stretching bands of trans ligands are evidenced at 537 and 519 cm^{-1} respectively. According to a D_{4h} symmetry of the ZrO_4F_2 unit, only the symmetric vibration should be Raman active. Actually, this was the case of the highly symmetric zirconium derivative that we recently obtained and characterized (ZPIP in ref 3f): a single band at 544 cm^{-1} was observed and assigned to the trans $F_\alpha ZrF_\beta$ symmetric stretching. However, due to the presence of the carboxylate group in *cis* position with respect to F atoms, a symmetry lowering (C_{2v}) can be assumed for **1a**, thus allowing both symmetric and asymmetric modes to be detected with the

Table 2. Carboxylate and Zr−F Stretching Modes: IR and Raman Frequencies[a]

compound	vibration	IR (cm^{-1})	Raman ($\Delta\nu/cm^{-1}$)
1	ν (C═O)	1736.4	1734.3
	ν (C−O)	1269.9	1269.2
	ν s ($F_\alpha ZrF_\beta$)	(557.5)[b]	551.5
	ν as ($F_\alpha ZrF_\beta$)	(530.0)	530.0
	ν (Zr − F_γ)	(498.3)	504.3
1a	ν (C═O)	1672.6	1669.4
	ν (C−O)	1341.7	1332.6
	ν s ($F_\alpha ZrF_\beta$)	(518.0)	519.0[c]
	ν as ($F_\alpha ZrF_\beta$)	(536.0)	537.0
2	ν (C═O)	1660.4	1664.6
	ν (C−O)	1373.5	1374.0
	ν s ($F_\alpha ZrF_\gamma$)	(560.0)	553.0
	ν as ($F_\alpha ZrF_\gamma$)	(531.0)	525.0

[a] ν: stretching mode; ν s: symmetric stretching; ν as: asymmetric stretching; α, β, and γ indexes refer to Figure 9. [b] Due to the overlapping with Zr−O vibrations,[10] O−C−O and O−C−C deformations of nicotinic and isonicotinic units,[11] the assignment of low frequency IR absorptions is tentatively proposed in brackets after comparison with Raman bands. [c] Following the normal coordinate assignment of ref 13b, the symmetric stretching frequency of the trans-difluorine compound is lower than asymmetric counterpart; in the other two derivatives one has the opposite.

dx.doi.org/10.1021/cg301042y | *Cryst. Growth Des.* XXXX, XXX, XXX−XXX

absorption and the scattering techniques. Two Raman bands at 547 and 525 cm^{-1} are also measured for the nicotinic derivative. As well as the previous case, the symmetric and asymmetric stretching of Zr−F bonds are both Raman and IR active due to the low symmetry of the metal coordination structure (C_s), and a 20 cm^{-1} separation is measured between the two spectral components. Notwithstanding these similarities, a different position of Raman bands suggests different sites of F ligands in the coordination shell of Zr. In fact, the results obtained for **2** could support the assignment to a *cis* arrangement of fluorine ligands, in agreement with the situation already observed for Pt−F compounds.[14]

Solid-State NMR. ^{1}H and ^{19}F MAS spectra were recorded at quite high spinning speeds.

In particular, ^{1}H MAS spectra, reported in Figure 11, show a very poor spectral resolution, indicating that MAS can only slightly reduce the strong $^{1}H-^{1}H$ dipolar interactions, typical of a very rigid organic structure. By looking closely at the spectra, it is possible to see that the spectra of **1a** and **2** are very similar, and, as far as the "resolved" part of the spectrum is concerned, they consist of a superposition of some broad peaks in the aliphatic and aromatic regions. On the contrary, the spectrum of **1** looks quite different, and it clearly shows a peak at about 12 ppm, which can be straightforwardly assigned to the acidic proton of the HF group, and which is not present in the spectra of **1a** and **2**. This observation is in full agreement with the hypothesized structures for **1**, **1a**, and **2**, especially with the loss of a molecule of HF on heating sample **1** to give **1a**. The detailed interpretation of the rest of the spectrum is not trivial considering the very poor spectral resolution.

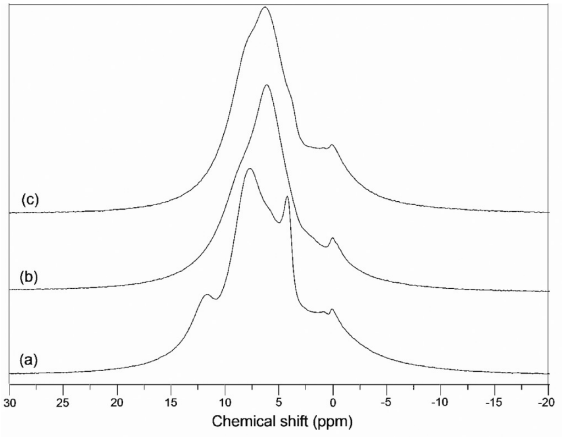

Figure 11. The ^{1}H MAS spectra of **1** (a), **1a** (b), and **2** (c). The spectra were recorded at a MAS spinning frequency of 22 kHz.

^{19}F MAS spectra, reported in Figure 12, show the typical patterns arising by the presence of many spinning sidebands. In this case, contrary to ^{1}H MAS spectra, we could achieve a good spectral resolution since ^{19}F nuclei are affected by weaker homonuclear ($^{19}F-^{19}F$) and heteronuclear ($^{19}F-^{1}H$) dipolar interactions than ^{1}H nuclei. The main cause of line broadening is reasonably ^{19}F chemical shift anisotropy, which, due to its inhomogeneous character, is strongly affected by MAS, which gives rise to quite narrow isotropic peaks and spinning sidebands. Furthermore, possible residual homo- and heteronuclear dipolar coupling should also have a main inhomogeneous character, as arising from two-body couplings, considering the absence of an extended network of tightly coupled

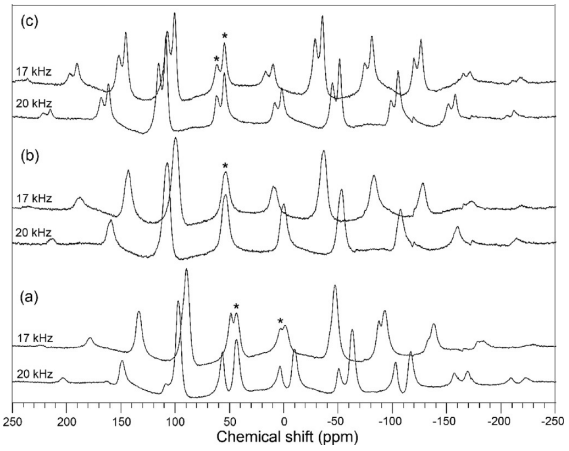

Figure 12. The ^{19}F MAS spectra of **1** (a), **1a** (b), and **2** (c). The isotropic peaks are marked with stars. The spectra were recorded at MAS spinning frequencies of 17 and 20 kHz, as indicated in the figure.

nuclei. In order to identify isotropic peaks, distinguishing them from spinning sidebands, we recorded many spectra at different MAS frequencies (in the figure only those at 17 and 20 kHz are reported). Indeed, while isotropic peaks do not change their resonance position with the MAS frequency, spinning sidebands do. It is possible to observe from the spectra that 2, 1, and 2 isotropic peaks can be identified for **1**, **1a**, and **2**, respectively. In particular, in **1** the two isotropic peaks resonate at about 3 and 44 ppm: by taking into account the integrals of isotropic peaks and all sidebands it is possible to estimate a 1:2 ratio between the two groups of signals, indicating that one of the three fluorine atoms in the molecular structure is responsible for the signal with an isotropic chemical shift of 3 ppm, while that at 44 ppm arises from two fluorine atoms. On the basis of molecular structure and symmetry the assignment is quite straightforward, the two signals corresponding to the equatorial (F_γ) and axial (F_α and F_β) fluorine atoms, respectively. In **1a** there is only one distinguishable group of peaks, with an isotropic chemical shift of about 54 ppm. On one side, this strongly supports the loss of the equatorial fluorine atom (as HF) following heating of **1**, and on the other side it reveals a non-negligible change of chemical environment for the axial fluorine atoms as a consequence of the structural rearrangement. In **2**, two groups of peaks slightly differing for their isotropic chemical shift (55 and 62 ppm) are observed. Again, taking into account the integrals of the isotropic peaks and all the sidebands, the ratio between the corresponding fluorine atoms is 1:1, although the two groups of signals exhibit clearly different linewidths. These two groups of signals can in principle be assigned to either the two fluorine atoms in the molecular structure (which are indeed slightly inequivalent because of geometrical distortions from the perfect octahedral structure) or the two different molecules in the unit cell, as revealed by the X-ray analysis. Although this doubt cannot be unequivocally solved at the current stage, by looking at samples **1** and **1a**, where small geometrical distortions do not give rise to a detectable NMR inequivalence, we believe that in **2** the two signals should be ascribed to the two distinct molecules in the unit cell. It must be noticed that these two signals show a clearly different line width, which could arise from different residual $^{19}F-^{1}H$ dipolar couplings, probably resulting from a different exposure of the two fluorine atom pairs to the neighboring organic chains.

dx.doi.org/10.1021/cg301042y | *Cryst. Growth Des.* XXXX, XXX, XXX−XXX

CONCLUSIONS

The information provided by the joint use of PXRD, FT-IR, Raman, and solid-state NMR allowed us to draw a clear picture of the phase transition occurring in **1**, involving the loss of HF and the consequent rearrangement of the structure to fill the coordination vacancy created on the zirconium atom. The result was the covalent joining of the 1D chains constituting **1** to yield the 2D hybrid layers of **1a**. The latter is a polymorph of **2**, which is a 2D compound too, only based on a geometrical isomer of the building block present in **1a**. Notably, **2** represents a new structural archetype.

Besides the good results obtained, this work represents a first example of a thorough study of zirconium phosphonates via solid-state NMR, so we are planning to extend this kind of characterization to other compounds of the same class. At the same time, vibrational spectroscopy was also confirmed to be a powerful tool for the description of some structural details, as we already showed in a previous work.

ASSOCIATED CONTENT

Supporting Information

Crystallographic information file for **1**, **1a**, and **2** (CIF). Tables with complete crystallographic parameters for **1**, **1a**, and **2.** Additional figures. This material is available free of charge via the Internet at http://pubs.acs.org.

AUTHOR INFORMATION

Corresponding Author

*E-mail: marcotaddei@hotmail.com.

Notes

The authors declare no competing financial interest.

ACKNOWLEDGMENTS

The authors thank Dr. Claudia Forte for helpful discussion. This work was supported by MIUR - Project FIRB 2010 No. RBFR10CWDA_003.

REFERENCES

(1) (a) Clearfield, A. In *Progress in Inorganic Chemistry*; Karlin, K. D., Ed.; John Wiley & Sons: New York, 1998; Vol. *47*, pp 374−510; (b) Vivani, R.; Alberti, G.; Costantino, F.; Nocchetti, M. *Microporous Mesoporous Mater.* **2008**, *107*, 58−70. (c) Vivani, R.; Costantino, F.; Taddei, M. In *Metal Phosphonate Chemistry: From Synthesis to Applications*; Clearfield, A.; Demadis, K., Eds.; Royal Society of Chemistry: Oxford, 2011; Chapter 2.

(2) (a) Alberti, G.; Casciola, M. *Solid State Ionics* **2001**, *145*, 3−16. (b) Alberti, G.; Casciola, M.; D'Alessandro, E.; Pica, M. *J. Mater. Chem.* **2004**, *14*, 1910−1914. (c) Curini, M.; Rosati, O.; Costantino, U. *Curr. Org. Chem.* **2004**, *8*, 591−606. (d) Donnadio, A.; Pica, M.; Taddei, M.; Vivani, R. *J. Mater. Chem.* **2012**, *22*, 5098−5106. (e) Queffélec, C.; Petit, M.; Janvier, P.; Knight, D. A.; Bujoli, B. *Chem. Rev.* **2012**, *112*, 3777−3807.

(3) (a) Costantino, U.; Nocchetti, M.; Vivani, R. *J. Am. Chem. Soc.* **2002**, *124*, 8428−8434. (b) Vivani, R.; Costantino, U.; Nocchetti, M. *J. Mater. Chem.* **2002**, *12*, 3254−3260. (c) Vivani, R.; Costantino, F.; Nocchetti, M.; Gatta, G. D. *J. Solid State Chem.* **2004**, *177*, 4013−4022. (d) Vivani, R.; Costantino, F.; Costantino, U.; Nocchetti, M. *Inorg. Chem.* **2006**, *45*, 2388−2390. (e) Taddei, M.; Costantino, F.; Vivani, R. *Inorg. Chem.* **2010**, *49*, 9664−9670. (f) Taddei, M.; Costantino, F.; Manuali, V.; Vivani, R. *Inorg. Chem.* **2011**, *50*, 10835−10843.

(4) (a) Vermeulen, L. A.; Thompson, M. E. *Nature* **1992**, *358*, 656−658. (b) Vermeulen, L. A.; Thompson, M. E. *Chem. Mater.* **1994**, *6*, 77−81. (c) Poojary, D. M.; Vermeulen, L. A.; Vicenzi, E.; Clearfield, A.; Thompson, M. E. *Chem. Mater.* **1994**, *6*, 1845−1849. (d) Vermeulen, L. A.; Snover, J. L.; Sapochak, L. S.; Thompson, M. E. *J. Am. Chem. Soc.* **1993**, *115*, 11767−11774. (e) Byrd, H.; Clearfield, A.; Poojary, D. M.; Reis, K. P.; Thompson, M. E. *Chem. Mater.* **1996**, *8*, 2239−2246. (f) Vermeulen, L. A.; Burgmeyer, S. J. *J. Solid State Chem.* **1999**, *147*, 520−526. (g) Vermeulen, L. A.; Fateen, R. Z.; Robinson, P. D. *Inorg. Chem.* **2002**, *41*, 2310−2312.

(5) Werner, P. E.; Eriksson, L.; Westdhal, M. *J. Appl. Crystallogr.* **1985**, *18*, 367−370.

(6) Laugier, J.; Bochu, B. *LMGP-Suite*; ENSP/Laboratoire des Materiaux et du Genie Physique: 38042 Saint Martin d'Heres, France, 2002.

(7) Favre-Nicolin, V.; Cerny, R. *J. Appl. Crystallogr.* **2002**, *35*, 734−743.

(8) Falcioni, M.; Deem, M. W. *J. Chem. Phys.* **1999**, *110*, 1754−1767.

(9) Larson, C.; von Dreele, R. B. *Generalized Crystal Structure Analysis System*; Los Alamos National Laboratory, New Mexico, 2001.

(10) (a) Demadis, K. D.; Papadaki, M.; Aranda, M. A. G.; Cabeza, A.; Olivera-Pastor, P.; Sanakis, Y. *Cryst. Growth Des.* **2010**, *10*, 357−364. (b) Colodrero, R. M. P.; Olivera-Pastor, P.; Cabeza, A.; Papadaki, M.; Demadis, K. D.; Aranda, M. A. G. *Inorg. Chem.* **2010**, *49*, 761−768. (c) Demadis, K. D.; Famelis, N.; Cabeza, A.; Aranda, M. A. G; Colodrero, R. M. P.; Infantes-Molina, A. *Inorg. Chem.* **2012**, *51*, 7889−7896.

(11) Stanghellini, P. L.; Boccaleri, E.; Diana, E.; Alberti, G.; Vivani, R. *Inorg. Chem.* **2004**, *43*, 5698−5703.

(12) Socrates, G. *Infrared and Raman Characteristic Group Frequencies − Tables and Charts*; John Wiley and Sons Ltd.: Chichester UK, 2001.

(13) Nakamoto, K. *Infrared and Raman Spectra of Inorganic and Coordination Compounds*; John Wiley and Sons Ltd.: Hobonek NJ, 2009.

(14) (a) Erlhöfer, P.; Preetz, W. *Z. Natuforsch.* **1989**, *44b*, 412−418. (b) Erlhöfer, P.; Preetz, W. *Z. Natuforsch.* **1989**, *44b*, 1214−1220.